An Improved Repetitive Control of DFIG-DC System for Torque Ripple Suppression

Chao Wu and Heng Nian, *Senior Member, IEEE*

***Abstract*—In order to obtain smooth torque and output power of the doubly fed induction generator (DFIG) dc system in which an uncontrollable rectifier is used to connect the stator winding and dc grid, an improved repetitive control (RC) regulator is proposed for the rotor-side converter to suppress the torque ripple in this paper. The torque control of the DFIG is divided into the average torque control and the torque ripple control. For the average torque control, a novel stator frequency estimation method is proposed to acquire the frequency and angle of the stator flux linkage. Then, the stator flux linkage orientation is applied for the decoupling control of the stator frequency and average torque. For the torque ripple control, an improved RC regulator is designed and directly employed for suppressing the torque ripple completely, which can avoid the sequence decomposition and rotor harmonic current calculation. The detailed design of the improved RC regulator is presented considering the control bandwidth, the fractional delay, and suppressing of the infinite dc gain. Finally, the proposed control method is validated by the experiment results.**

***Index Terms*—DC grid, doubly fed induction generator (DFIG), repetitive control (RC), torque ripple suppression.**

NOMENCLATURE

$\boldsymbol{U}$	Stator or rotor voltage.
$\boldsymbol{I}$	Stator or rotor current.
P	Stator or rotor power.
$\boldsymbol{\psi}$	Stator or rotor flux linkage.
L_s, L_m, L_r	Stator, mutual, and rotor inductances, respectively.
R_s, R_r	Stator and rotor resistances, respectively.
n_p	Number of pole pairs.
T_e	Electromagnetic torque.
$L_{s\sigma}, L_{r\sigma}$	Stator and rotor leakage inductances, respectively.
ω_s, ω_r	Stator frequency and rotor speed, respectively.
ω_{s1}, ω_{sh}	Fundamental frequency and harmonic frequency, respectively.
sl_1, sl_h	Slip rates of the fundamental and harmonic circuit, respectively.
G_{CRC}	Conventional RC regulator.
G_{BRC}	RC regulator with bandwidth.
G_{IRC}	Improved RC regulator.
k_{RC}	Gain of RC regulator.
G_{hp}	High-pass regulator.

Subscripts

d, q	Variables on a rotating reference frame.
s, r	Stator and rotor quantities, respectively.

Superscripts

$*$	Reference value.
Δ	Rotor quantities relative to the Γ circuit.
$\wedge$	Estimated value.

Manuscript received June 8, 2017; revised August 20, 2017; accepted October 23, 2017. Date of publication October 25, 2017; date of current version June 22, 2018. This work was supported in part by the National Natural Science Foundation of China under Grant 51622706, and in part by the Fundamental Research Funds for the Central Universities under Grant 2017XZZX002-17. Recommended for publication by Associate Editor R. Burgos. *(Corresponding author: Heng Nian.)*

The authors are with the College of Electrical Engineering, Zhejiang University, Hangzhou 310027 China (e-mail: superwu@zju.edu.cn; nianheng@zju.edu.cn).

Color versions of one or more of the figures in this paper are available online at http://ieeexplore.ieee.org.

Digital Object Identifier 10.1109/TPEL.2017.2766886

I. INTRODUCTION

NOWADAYS, the number of offshore wind farms (OWFs) based on the doubly fed induction generator (DFIG) is increasing rapidly; these usually are distant from the onshore grid. Conventional high voltage alternating current transmission is not flexible and the capacity is limited due to large charging currents of the cables [1]–[5]. One effective alternative is to apply the high voltage direct current transmission for the large capacity OWFs. Thus, it is of significant importance to investigate the topology and control strategy for a DFIG-based wind turbine connected to a dc grid.

The DFIG-DC system, based on a single derated pulse width modulation (PWM) converter on the rotor side and a fully rated uncontrolled rectifier on the stator side, has been extensively investigated due to the reduced cost and simple configuration of the power converter [6]–[13]. The rotor-side converter (RSC) and the stator-side diode bridge are connected to the same dc link, as can be seen in Fig. 1.

There are mainly two operation modes of this DFIG-DC system in the existed literature [6]–[17]. The first one is applied for the dc grid connected condition, in which the dc voltage is constant and the DFIG works as a power source [6]–[14]. By controlling the RSC, the DFIG can output power to the dc grid through the stator-side diode bridge. The second one is operated as the stand-alone operation mode, in this condition, the dc voltage is not constant and the primary objective is to control the dc voltage [15]–[17]. In this paper, the dc grid connected DFIG-DC system is investigated, thus the dc voltage is constant in this paper and the control objective is to achieve smooth and steady torque and power of DFIG in this condition. Some control schemes specifically devoted to the DFIG-DC systems connected to the dc grid have been recently studied in [6]–[14].

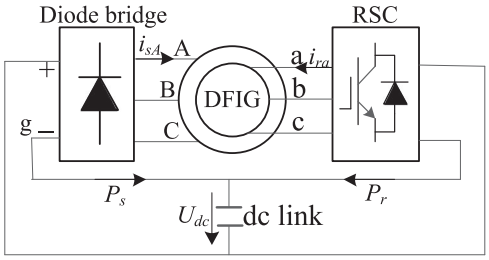

Fig. 1. Configuration of a DFIG-DC system.

First, the basic operation and design issues of the DFIG-DC system were initially studied in [6], which presented a decoupling control method to regulate the torque and the stator frequency of DFIG. In [7]–[9], the stator voltage is used to calculate the angle of the stator flux linkage for the orientation in the control strategy, which needs the stator voltage sensor. In [10] and [11], the sersorless operation of the DFIG-DC system is investigated to avoid the rotor position sensor, in which the stator voltage is applied in the phase-locked loop (PLL) for estimating the stator frequency. In the above-mentioned literature, only a fundamental frequency circuit is modeled to implement the control of the average torque, and the torque ripple caused by the harmonic components of voltage and current is ignored. In order to reduce the torque ripple, a resonant controller was added in the current loop to track the rotor current references of six times frequency in [12], and a direct resonant control strategy is applied for mitigating the torque ripple in [13], in which only the sixth-order harmonic component is considered. Furthermore, a torque ripple mitigation strategy based on a predictive estimation of the reciprocal of flux linkage is proposed in [14], which avoids applying periodic control techniques. Thus, the predictive delay compensation method is very robust against stator frequency variations. However, since the stator voltage is a step wave when the stator winding is connected to the diode rectifier, the harmonic components are abundant in the stator voltage, which would cause highly distorted stator and rotor currents and cause torque and power ripple correspondingly.

In conclusion, the basic control of the stator frequency and the average torque of the DFIG-DC system have been extensively investigated in the literature. However, there are still some drawbacks of the existed control strategies, which are as follows:

1) The stator voltage is highly distorted, which is not suitable for the calculation of the stator frequency and the angle of stator flux linkage. However, since the stator flux linkage is an integration of the stator voltage, the stator flux linkage is more appropriate for estimating the stator frequency and orientation angle.
2) Only the torque ripple caused by 5th and 7th harmonics are considered, however, the higher order harmonics such as 11th, 13th, 17th, and 19th harmonics also should be considered since the stator voltage is a step wave. Thus, the suppression method of the torque ripple needs to be improved. When considering higher order harmonic components in the torque, such as 12th and 18th order, a large number of paralleled resonant controllers should be employed, which might cause heavy parallel computation burden and tuning complexity [14]. Based on the internal model principle, repetitive control (RC) can achieve zero steady-state error tracking of any periodic harmonic components due to the introduction of high gains at the interested harmonic frequencies [15]–[18], which offers accurate control solutions to suppress the torque ripple.
3) In order to reduce the torque ripple, the conventional method is to calculate the rotor harmonic current reference and apply the resonant controllers tracking the rotor harmonic current. The RC regulator is plugged in the rotor current loop. In order to avoid calculating the rotor harmonic current reference, the torque error is directly applied as the input of the RC regulator, and the output of RC regulator is considered as the corresponding harmonic voltage reference, which is defined as the direct RC in this paper.

In this paper, the torque control of the DFIG is divided into the average torque control and the torque ripple control. For the average torque control, a novel stator frequency estimation method is proposed without using the distorted stator voltage. Then, the angle of stator flux linkage is applied as the orientation angle to achieve the accurate decoupling control of the stator frequency and average torque based on proportional-integral (PI) controller.

For the suppression of torque ripple, the direct RC is applied to produce appropriate rotor harmonic voltage compensation. In this way, the calculation of the rotor harmonic current references can be avoided, which would prominently reduce the complexity of the control strategy and improve the robustness against the parameter deviations.

The rest of this paper is organized as follows. The system configuration and mathematical model are outlined in Section II. The control strategy of an RSC and the design of the improved RC regulator are elaborated in detail in Section III. Furthermore, the performance analysis of the proposed control strategy is presented in Section IV. Section V shows the experimental results. Finally, the conclusion is made in Section VI.

II. System Layout and Mathematical Model

A. System Layout

The DFIG system connected to the dc link is shown in Fig. 1, in which the stator is connected to the dc link through the diode rectifier and the rotor is connected through a PWM converter. The reference direction of the stator and rotor currents is shown in Fig. 1. Differently from the conventionally ac grid connected DFIG, the grid-side converter can be avoided.

Fig. 2 shows the Γ equivalent circuit of DFIG in the steady state. When the stator flux linkage orientation method is adopted, the Γ equivalent circuit can be divided into the exciting circuit and the power circuit. The exciting current flows through the exciting circuit, which can generate the appropriate stator voltage for conducting the diode bridge. The active power current flows through the power circuit, which can regulate the electromagnetic torque and the output power to the dc grid.

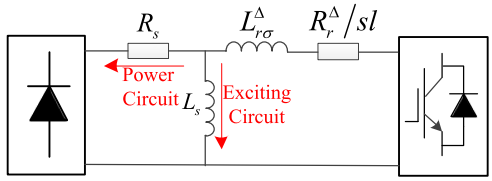

Fig. 2. Equivalent circuit of a DFIG connected to dc link.

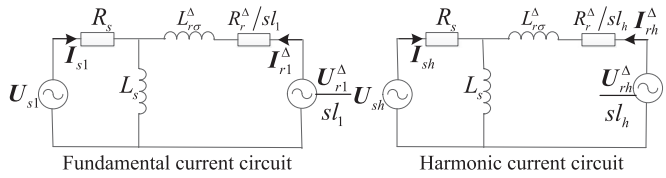

Fig. 3. Equivalent fundamental and harmonic circuit of a DFIG.

When the diode rectifier operates at the continuous conduction mode, the stator voltage is clamped to the three-step square wave, which can be expressed by the Fourier transformation as follows:

$$U_{sa}(t)=\frac{2}{\pi}U_{dc}\left(\sin\omega t+\sum_{n=1}^{\infty}\left(\frac{\sin(6n-1)\omega t}{6n-1}+\frac{\sin(6n+1)\omega t}{6n+1}\right)\right). \tag{1}$$

Due to the highly distorted stator voltage, the stator currents and rotor currents are highly distorted, which would cause the power and torque ripple. In the existed control strategy for reducing torque ripple of DFIG-DC system, only the torque ripple caused by fifth and seventh harmonic voltages are considered [12], [13]. However, the high-order harmonics, such as eleventh, thirteen, seventeen, and nineteen harmonics, also should be considered since the stator voltage is a step wave. In this paper, the stator fundamental voltage and the harmonic voltages are all considered. The fundamental voltage is considered in the fundamental current circuit and the harmonic voltages are considered in the harmonic current circuit.

In the steady state, the stator and rotor voltages and flux linkage in the stator reference frame can be expressed as

$$\begin{cases}\boldsymbol{U}_{sdq}=R_s\boldsymbol{I}_{sdq}+j\omega_s\boldsymbol{\psi}_{sdq}\\ \frac{\boldsymbol{U}^{\Delta}_{rdq}}{sl}=\frac{R^{\Delta}_r}{sl}\boldsymbol{I}^{\Delta}_{rdq}+j\omega_s L^{\Delta}_{r\sigma}\boldsymbol{I}^{\Delta}_{rdq}+j\omega_s\boldsymbol{\psi}^{\Delta}_{rdq}\\ sl=\frac{\omega_s-\omega_r}{\omega_s},\ L^{\Delta}_{r\sigma}=\left(\frac{L_s}{L_m}\right)^2L_r-L_s\end{cases} \tag{2}$$

$$\begin{cases}\boldsymbol{\psi}_{sdq}=L_s\boldsymbol{I}_{sdq}+L_m\boldsymbol{I}_{rdq}\\ \boldsymbol{\psi}_{rdq}=L_m\boldsymbol{I}_{sdq}+L_r\boldsymbol{I}_{rdq}\end{cases} \tag{3}$$

$$R^{\Delta}_r=\left(\frac{L_s}{L_m}\right)^2R_r,\ \boldsymbol{U}^{\Delta}_r=\frac{L_s}{L_m}\boldsymbol{U}_r,\ \boldsymbol{I}^{\Delta}_{rdq}=\frac{L_m}{L_s}\boldsymbol{I}_{rdq} \tag{4}$$

where $\boldsymbol{U}$ is the voltage, R_s and R_r are stator and rotor resistances, respectively, ω_s is the stator frequency, ω_r is rotor angular speed, sl is the slip ratio, $\boldsymbol{\psi}$ is the flux, $\boldsymbol{I}$ is the current, $L_s=L_m+L_{s\sigma}$ and $L_r=L_m+L_{r\sigma}$ are the self-inductances of stator and rotor windings, respectively, $L_{s\sigma}$ and $L_{r\sigma}$ are stator and rotor leakage inductances, respectively, L_m is the mutual inductance; subscripts s, r represent the stator and rotor, respectively, subscripts d, q represent components at the $d-q$ axes, respectively, and superscript Δ represents rotor quantities relative to the Γ equivalent circuit.

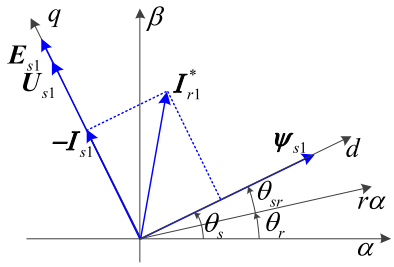

Fig. 4. Phasor diagram of a fundamental current circuit in the steady state.

B. Fundamental and Harmonic Equivalent Circuit

In order to analyze the influence of distorted stator voltage on the operation performance of DFIG, the equivalent circuit of DFIG is divided into fundamental current circuit and harmonic current circuit [19]. The fundamental current circuit is applied for the stator frequency control and average torque control, which guarantees the power tracking operation of DFIG connected to dc link through a diode bridge on the stator. For the harmonic current circuit, the rotor harmonic voltages are also injected to the rotor side for suppressing the torque ripple. The equivalent fundamental and harmonic circuit of the DFIG is shown in Fig. 3, where $sl_1=\frac{\omega_{s1}-\omega_r}{\omega_{s1}}$ and $sl_h=\frac{\omega_{sh}-\omega_r}{\omega_{sh}}$

Fig. 4 shows the phasor diagram of the fundamental current circuit when the stator flux linkage orientation is applied.

As can be seen from (1), the distorted stator voltage of DFIG in the dq reference frame can be expressed as

$$\boldsymbol{U}^{+}_{sdq}=\boldsymbol{U}^{+}_{sdq+}+\sum_{n=1}^{\infty}\left(\boldsymbol{U}^{(6n-1)-}_{sdq(6n-1)-}e^{-j6n\theta_1}+\boldsymbol{U}^{(6n+1)+}_{sdq(6n+1)+}e^{j6n\theta_1}\right). \tag{5}$$

Then, the stator current of DFIG under the distorted stator voltage can be expressed as

$$\boldsymbol{I}^{+}_{sdq}=\boldsymbol{I}^{+}_{sdq+}+\sum_{n=1}^{\infty}\left(\boldsymbol{I}^{(6n-1)-}_{sdq(6n-1)-}e^{-j6n\theta_1}+\boldsymbol{I}^{(6n+1)+}_{sdq(6n+1)+}e^{j6n\theta_1}\right) \tag{6}$$

where superscripts $+$, $(6n-1)-$, and $(6n+1)+$ represent the reference frames rotating at the fundamental angular speed in the positive direction, at the angular speed of $(6n-1)$ times of fundamental angular speed in the negative direction, and at the angular speed of $(6n+1)$ times of fundamental angular speed in the positive direction, respectively; subscripts $+$,

$(6n-1)-$, and $(6n+1)+$ represent the fundamental and harmonic components, i.e., 5th, 7th, 11th, 13th, 17th, 19th, etc., and θ_1 represents the phase angle of stator fundamental flux linkage.

As can be seen from the stator voltage expression in (5), the stator flux can be expressed as

$$\boldsymbol{\psi}^{+}_{sdq} = \boldsymbol{\psi}^{+}_{sdq+} + \sum_{n=1}^{\infty}\left(\boldsymbol{\psi}^{(6n-1)-}_{sdq(6n-1)-}e^{-j6n\theta_1} + \boldsymbol{\psi}^{(6n+1)+}_{sdq(6n+1)+}e^{j6n\theta_1}\right) \tag{7}$$

where

$$\boldsymbol{\psi}^{(6n-1)-}_{sdq(6n-1)-} = \frac{\boldsymbol{U}^{(6n-1)-}_{sdq(6n-1)-}}{-j(6n-1)\omega_1}, \boldsymbol{\psi}^{(6n+1)+}_{sdq(6n+1)+} = \frac{\boldsymbol{U}^{(6n+1)+}_{sdq(6n+1)+}}{j(6n+1)\omega_1}$$

As can be seen from (7), the harmonic components in the stator flux linkage are smaller than the stator voltage. Then, the stator active power and the electromagnetic torque can be expressed as

$$P_s = \frac{3}{2}Re\left(\boldsymbol{U}^{+}_{sdq}\boldsymbol{I}^{+}_{sdq}\right) = P_{s0} + \sum_{n=1}^{\infty}P_{s6n} \tag{8}$$

$$P_r = \frac{3}{2}Re\left(\boldsymbol{U}^{+}_{rdq}\boldsymbol{I}^{+}_{rdq}\right) = P_{r0} + \sum_{n=1}^{\infty}P_{r6n}. \tag{9}$$

The total power from the DFIG to the dc grid is the sum of the stator power and the rotor power, which can be expressed as

$$P_t = P_s + P_r \approx \omega_r T_e. \tag{10}$$

It can be seen that when the torque ripple is eliminated, the ripple of the total output power can also be eliminated. Thus, the suppression of torque ripple is not only beneficial for the operation of the DFIG but also for the power transmission to the dc grid.

Therefore, the main objective of the proposed control strategy is to suppress the torque ripple completely. The torque can be represented as

$$T_e = \frac{3}{2}n_p Re\left(j\boldsymbol{\psi}^{+}_{sdq}\hat{\boldsymbol{I}}^{+}_{sdq}\right) = \frac{3}{2}n_p L_m\left(I_{sd}I_{rq} - I_{sq}I_{rd}\right) = T_{e0} + \sum_{n=1}^{\infty}T_{e6n} \tag{11}$$

where T_{e0} is the average torque and sum of T_{e6n} is the torque ripple.

Combining (7) and (9), the torque ripple can be expressed by the stator voltage and stator current

$$T_{e6n} = \frac{3n_p}{2\omega_{s1}}R_e \left[\begin{array}{l}\left(\boldsymbol{U}^{+}_{sdq+}\hat{\boldsymbol{I}}^{(6n+1)+}_{sdq(6n+1)+} - \frac{\boldsymbol{U}^{(6n-1)-}_{sdq(6n-1)-}\hat{\boldsymbol{I}}^{+}_{sdq+}}{6n-1}\right)e^{-j6n\theta_1} \\ +\left(\boldsymbol{U}^{+}_{sdq+}\hat{\boldsymbol{I}}^{(6n-1)-}_{sdq(6n-1)-} + \frac{\boldsymbol{U}^{(6n+1)+}_{sdq(6n+1)+}\hat{\boldsymbol{I}}^{+}_{sdq+}}{6n+1}\right)e^{j6n\theta_1}\end{array}\right]. \tag{12}$$

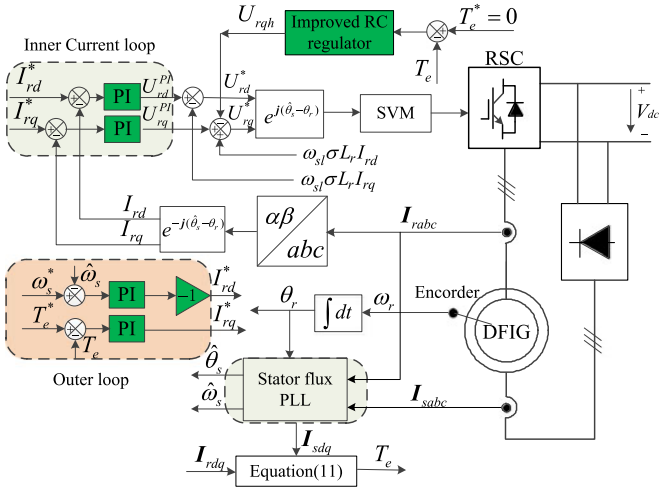

Fig. 5. Control scheme of an RSC based on the improved RC regulator.

As seen from (12), the torque ripple contains many items that are the product of the stator voltage and stator current at different frequencies. It is complex to calculate the rotor harmonic current reference from (12) to suppress the harmonic components of the torque. Thus, the direct RC is applied to avoid the calculation of the current references, which will be elaborated in Section III.

III. Control Strategy

In the DFIG-DC system, the dc voltage is supposed to be constant since it is connected to the dc grid. Compared with the traditional ac grid connected DFIG, the stator voltage is not imposed by the ac grid, which leads to the stator frequency that needs to be controlled additionally. Furthermore, the stator voltage is distorted as three-step square wave when the rectifier is continuously conducted, which would cause torque ripple consisted of different harmonic components. Thus, the control strategy in this paper is divided into the average torque control and the torque ripple control.

For the average torque control, the most significant characteristic of the topology is that the product of the stator fundamental flux linkage and stator frequency is constant, which can be used to control the frequency of the stator winding.

For the torque ripple control, the improved RC regulator is employed to directly generate the rotor harmonic voltages to suppress the torque ripple accurately.

The RSC control scheme for the torque and frequency regulation is shown in Fig. 5. The regulation of the stator frequency and average torque is the outer loop and the regulation of the rotor current is the inner loop. The output of the stator frequency regulation loop is the d-axis reference of rotor current. The output of the average torque regulation loop is the q-axis reference of rotor current. Since the torque is regulated by the q-axis rotor voltage, the torque ripple can be directly regulated by applying the improved RC regulator to generate q-axis rotor harmonic voltages. The input of the RC regulator is the torque error and the output is rotor harmonic voltage that is directly added to the rotor voltage reference to suppress the torque ripple.

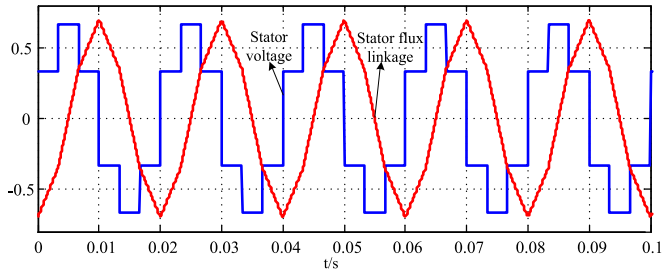

Fig. 6. Waveforms of stator voltage and stator flux linkage.

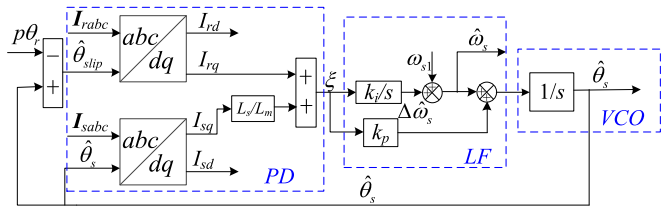

Fig. 7. Block of the stator flux PLL.

A. Stator Frequency and Average Torque Control

Since the stator frequency is a controlled variable of the DFIG-DC system, it is necessary to obtain the stator frequency of the DFIG. In [7] and [8], the stator voltage is employed to calculate the stator frequency directly based on the derivative of the angle of the stator flux linkage. In order to reduce the pulsation of the stator frequency, an enhanced PLL with a second-order low-pass filter based on stator voltage was applied for estimating the stator frequency [11]. The stator voltage is necessary in these methods. In this paper, a novel stator frequency estimating method is proposed and the influence of distorted stator voltage can be greatly reduced.

The novel stator frequency estimating method is proposed based on the stator flux linkage. When the stator voltage is a step wave, the waveforms of the stator voltage and stator flux linkage are shown in Fig. 6. As can be seen from the expression of stator flux linkage in (7), the harmonic components decrease progressively with the increasing frequency. Thus, the total harmonic distortion (THD) of the stator flux linkage is greatly smaller than the THD of stator voltage, the stator flux linkage is more appropriate for estimating the stator frequency. Instead of directly calculating the stator frequency, the stator frequency is indirectly obtained, and the stator flux linkage orientation is achieved by controlling the q-axis stator flux linkage to be zero. The block of the stator frequency estimating method and the stator flux linkage orientation is shown in Fig. 7.

It is well known that the PLL is mainly consisted of three parts, the phase discriminator (PD), loop filter (LF), and the voltage-controlled oscillator (VCO). The block of the stator frequency estimating method can be seen as the PLL of stator flux linkage. Instead of calculating the stator flux linkage from the voltage model, the current model is applied for calculating the stator flux linkage in the $d-q$ reference frame.

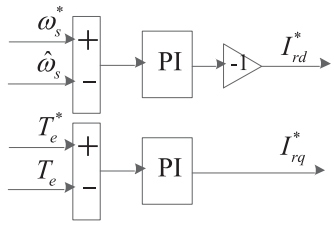

Fig. 8. Outer loop of the stator frequency and torque control.

The stator flux linkage in the $d-q$ frame can be expressed as

$$\begin{aligned}\boldsymbol{\psi}_{sd} &= L_s \boldsymbol{I}_{sd} + L_m \boldsymbol{I}_{rd} \\ \boldsymbol{\psi}_{sq} &= L_m \boldsymbol{I}_{sq} + L_r \boldsymbol{I}_{rq}.\end{aligned} \tag{13}$$

The output of the PD is the error between the actual angle of the stator flux linkage and the estimated angel, which can be expressed as

$$\xi = \frac{L_s}{L_m}\boldsymbol{I}_{sq} + \boldsymbol{I}_{rq}. \tag{14}$$

A PI regulator is used as the LF. Unlike the conventional PLL, the estimated stator frequency is not the output of the PI regulator but the output of the integrator only. In this way, the power step has little effect on the estimated stator frequency. The estimated phase angle is the output of the VCO, which is applied for the stator flux linkage orientation.

When the orientation angle error is regulated to be zero by the PI controller at the steady state, the estimated phase angle is the stator flux linkage angle and the estimated frequency is the stator frequency. Thus, the PLL of stator flux linkage is effective for estimating the stator frequency and orientation angle. The performance is better than the conventional stator voltage PLL, which will be validated by the experimental results presented in Section V.

If the stator flux linkage orientation is adopted, the q-axis stator flux linkage is zero and the amplitude of the stator flux linkage is depended on the d-axis current of stator and rotor. Moreover, the d-axis current of stator is almost zero because the phase displacement between the fundamental harmonics of the stator voltage and the stator current is generally small across the diode rectifier [10]. Thus, the d-axis current of rotor can be used to regulate the stator frequency, and the reference can be obtained from the outer loop of stator frequency control. The average torque is regulated by the q-axis current of current, and the q-axis rotor current reference can be obtained from the outer loop of torque control. The generation of the d-axis and q-axis rotor current reference is shown in Fig. 8.

B. Design and Analysis of Improved RC Regulator

For the purpose of eliminating the torque ripple of DFIG under the step wave stator voltage condition, the improved RC regulator is proposed to suppress the torque ripple directly. The fractional-order delay and the bandwidth of the repetitive controller are solved by improving the structure of the RC

appropriately. Furthermore, when the direct RC is applied, the abnormal PI part is compensated by the high-pass filter that the torque feedback in the harmonic control loop can be directly used in this paper.

1) Bandwidth of RC Regulator: First, due to the distorted stator voltage, the stator frequency will fluctuate around the average value. Thus, the bandwidth of the improved RC regulator needs to be designed in order to take consideration of the stator frequency deviation.

According to Marques and Iacchetti [14], the conventional RC (CRC) regulator can be presented as follows:

$$G_{CRC}(s) = \frac{k_{RC} e^{-T_0 s}}{1 - e^{-T_0 s}} \tag{15}$$

where k_{RC} is the gain parameter of CRC regulator, T_0 is the period of the fundamental control frequency, and $T_0 = 1/300$ s in this paper since the torque ripple includes harmonic components of 300, 600, 900 Hz, etc.

Moreover, based on the nature of exponential function, the conventional RC regulator given in (15) can also be written as

$$G_{CRC}(s) = -\frac{k_{RC}}{2} + \frac{k_{RC}}{T_0 s} + \frac{2k_{RC}}{T_0} \sum_{n=1}^{\infty} \frac{s}{s^2 + (n\omega_0)^2}. \tag{16}$$

From the aforementioned expression, it can be concluded that a repetitive controller is equivalent to a parallel combination of a negative proportional term, an integral element, and an infinite number of resonant controllers connected in parallel at harmonic frequencies. This implies that a repetitive controller contains lots of resonant frequencies, whereas a PR controller contains only one.

An ideal RC has infinite open-loop gain at resonant frequencies and can make the control system track the reference signals without steady-state error. However, it also results in poor stability inevitably and has poor robustness against the deviation of resonant frequencies. To improve the stability and robustness, a low-pass filter $Q(s)$ or a constant Q less than 1 is added to the internal model. When Q is a constant less than 1, the expression of RC regulator with bandwidth becomes

$$G_{BRC}(s) = \frac{k_{RC} Q e^{-T_0 s}}{1 - Q e^{-T_0 s}}. \tag{17}$$

Based on the nature of exponential function, (17) can be rewritten as

$$\begin{aligned} G_{BRC}(s) &= \frac{k_{RC} Q e^{-T_0 s}}{1 - Q e^{-T_0 s}} \\ &= -\frac{k_{RC}}{2} + \frac{k_{RC}}{T_0 s + T_0 \omega_c} + \frac{2k_{RC}}{T_0} \sum_{n=1}^{\infty} \frac{s + \omega_c}{s^2 + 2\omega_c s + \omega_c^2 + (n\omega_0)^2} \\ &\approx -\frac{k_{RC}}{2} + \frac{k_{RC}}{T_0 s + T_0 \omega_c} + \frac{2k_{RC}}{T_0} \sum_{n=1}^{\infty} \frac{s + \omega_c}{s^2 + 2\omega_c s + (n\omega_0)^2}. \end{aligned} \tag{18}$$

When ω_c is far smaller than ω_0, the symbol of approximate equal holds. ω_c is the resonant bandwidth and $\omega_c = -lnQ/T_0$. From (18), it can be seen that the integral element in (17) becomes an inertial element, and resonant controllers become quasi-resonant controllers. Therefore, it can be concluded that the modified RC with Q corresponds to a parallel combination of a negative proportional term, an inertial element, and a series of quasi-resonant controllers connected in parallel at harmonic frequencies.

2) Digital Implementation of RC Regulator: Since the RC regulator is implemented in the digital controller, it is essential to do an appropriate discretization of the RC regulator. Normally, the RC regulator with bandwidth in the discrete domain can be expressed as

$$G_{BRC}(z) = \frac{k_{RC} Q z^{-N}}{1 - Q e^{-N}} \tag{19}$$

where N is the ratio of sampling frequency f_s and the fundamental harmonic frequency f_0.

However, the sampling frequency is always 10 kHz and the fundamental harmonic frequency is 300 Hz, thus, it is inevitable that N is fractional, which cannot be directly implemented. The nearest integral of N is applied to substitute N which would cause high gains shift away from interested harmonic frequencies. According to the fractional delay (FD) filters design method [15], the FD z^{-N} can be well approximated by FD filters with integer orders. Assuming that $z^{-N} = z^{-N_i - F}$ with $N_i = int[N]$ being the integer part of N and $F = N - N_i$ $(0 < F < 1)$ being the fractional part of N, the FD z^{-F} can be approximated by a Lagrange interpolation polynomial FIR filter as

$$z^{-F} \approx \sum_{k=0}^{n} A_k z^{-k}, k = 0, 1, \ldots, n. \tag{20}$$

The coefficient A_k can be obtained as

$$A_k = \prod_{i=0, i \neq k}^{n} \frac{F - i}{k - i}, \quad k, i = 0, 1, \ldots, n. \tag{21}$$

Specifically, if $n = 1$ in (20), a linear interpolation polynomial $z^{-F} \approx (1 - F) + Fz^{-1}$ is used to approximate the FD part in [16]. However, in order to achieve a more accurate expression of the FD in the higher frequency, the bode diagram of the Lagrange-interpolation-based FIR filter with the order $n = 1, 2, 3$ is plotted in Fig. 9.

As can be seen from Fig. 9, the phase of the approximated FD filter is the same for $n = 1, 2, 3$ when the frequency is less than 1000 Hz. The magnitude response is closer to 1 with higher order. In this paper, the 300, 600, and 900 Hz are more concerned. If $n = 1$, the magnitude is 0.996, 0.984 and 0.964 at 300, 600, and 900 Hz, respectively. However, if $n = 2$, the magnitude is still 0.997 at 900 Hz without any appreciable attenuation. Thus, $n = 2$ is applied with a comprehensive consideration of accuracy and computational complexity.

When $n = 2$, the FD filter is approximated as

$$z^{-1/3} \approx 0.5556 + 0.5556z^{-1} - 0.1111z^{-2} = F(z). \tag{22}$$

In this way, the fractional repetitive controller with bandwidth in the discrete domain can be expressed as

$$G_{BRC}(z) = \frac{k_{RC} Q z^{-N_i} F(z)}{1 - Q e^{-N_i} F(z)}. \tag{23}$$

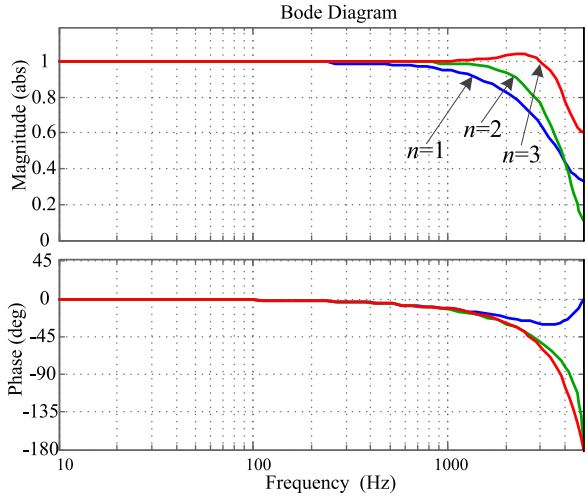

Fig. 9. Bode diagram of Lagrange-interpolation-based FIR filter with $n = 1, 2, 3$.

3) Suppressing Infinite DC Gain of CRC: Since the torque error also contains the average torque that is a dc component, the infinite gain of dc in a CRC regulator should be avoided. Then, a high-pass filter is added in the RC regulator to decrease the gain of dc part. Thus, the improved RC can be expressed as

$$G_{IRC}(z) = \frac{k_{RC} Q z^{-N_i} F(z) G_{hp}(z)}{1 - Q e^{-N_i} F(z)} \tag{24}$$

$$G_{hp}(s) = \frac{s}{s + 300\pi}. \tag{25}$$

The discretization method based on bilinearization is employed to obtain the high-pass filter in the discrete domain as

$$G_{hp}(z) = \frac{0.955z - 0.955}{z - 0.91}. \tag{26}$$

The bode diagram of the CRC regulator and the improved RC regulator is shown in Fig. 10. As can be seen from the figure, compared with the CRC regulator, the improved RC regulator eliminates the infinite dc gain, which is beneficial for the direct resonant control. Furthermore, the phase response of the improved RC leads that of the CRC by 180°, which is beneficial for stability of the control system. At the resonant harmonic frequencies, the gain of the improved RC does not reduce with the increase in frequency. And the bandwidth of the improved RC regulator is added to take account of the inaccuracy of the stator frequency.

C. Suppression of Torque Ripple

As can be seen from torque expression (12), the torque ripple consists of different harmonic frequency components. Thus, an improved RC regulator is employed for the torque ripple suppression. In this paper, the input of the improved RC regulator is the error of the torque, and the output is directly added to the rotor voltage reference. Thus, the sequential separations and complicated calculation of rotor current references can be avoided.

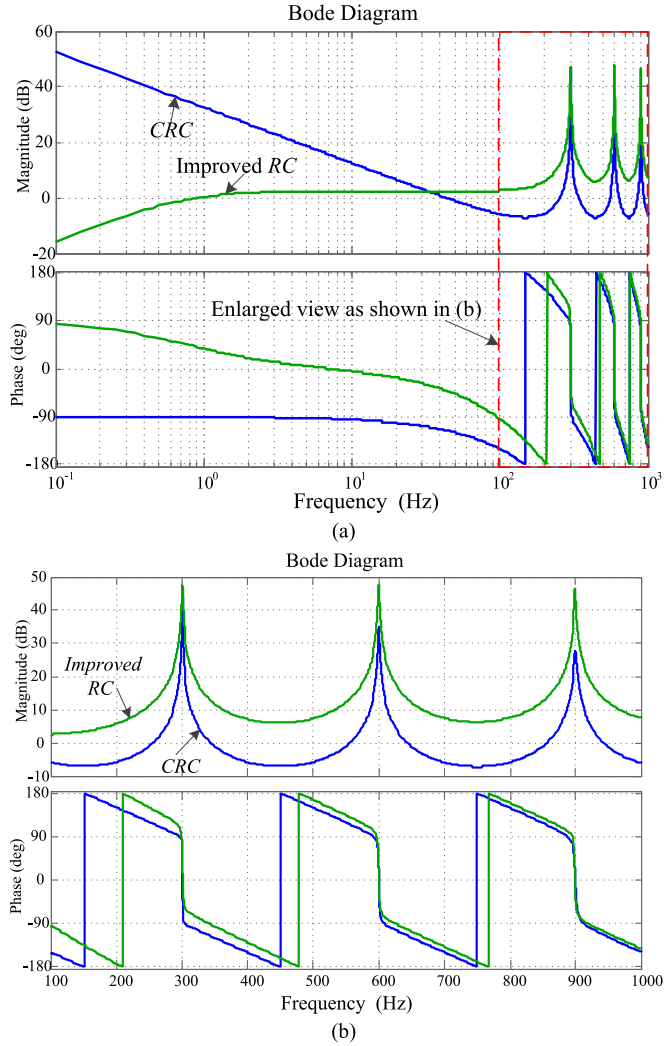

Fig. 10. Bode diagram of CRC and improved RC regulator.

The transfer function of the improved RC regulator in the discrete domain can be expressed as

$$G_{IRC}(z) = \frac{k_{RC} Q z^{-N_i} F(z) G_{hp}(z)}{1 - Q e^{-N_i} F(z)} \tag{27}$$

where k_{RC} is the gain of the improved RC regulator.

The bandwidth ω_c is applied to take account of the inaccuracy of the stator frequency, whose range is always designed from 5 to 20 rad/s [12]. The fundamental harmonic period $T_0 = 1/300$, thus when $\omega_c = 10$ rad/s, $Q = 0.9672$ and when $\omega_c = 5$ rad/s, $Q = 0.9835$.

Finally, the rotor voltage reference can be expressed as

$$\boldsymbol{U}^*_{rdq} = \boldsymbol{U}^{PI}_{rdq} - \boldsymbol{U}^{R}_{rdq} + j\sigma L_r \omega_{sl} \boldsymbol{I}_{rdq} \tag{28}$$

where $\boldsymbol{U}^{PI}_{rdq}$ is the output of the PI controller, $\boldsymbol{U}^{R}_{rdq}$ is the output of the torque resonant compensator, $j\sigma\omega_{sl}L_r I_{rdq}$ is the cross-coupling terms as feedforward item [12].

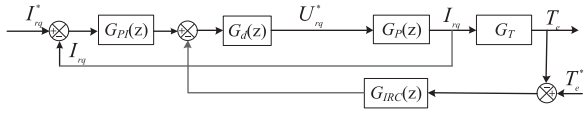

Fig. 11. Block diagram of the closed-loop control based on the proposed improved RC.

IV. System Analysis

A. Closed-Loop Control Stability Analysis

For the control loop of the stator frequency and average torque, the stability of the fundamental rotor current control has been validated in [13]. Thus, it is not repeated in this paper. As reported in the previous works [15]–[18], the RC regulator based control system may always suffer the instability operation, and even results in the failure of the DFIG control. It is critical to make sure that the proposed improved RC regulator would operate stably, so it is necessary to discuss the closed-loop control stability with different bandwidths ω_c and different gain parameters k_{RC}.

The control scheme of an RSC is shown in Fig. 5. The q-axis rotor reference current is the output of the torque PI controller. Since the torque PI controller is only in charge of the average torque regulation and its bandwidth is adequately low, which would not interact with the RC controller, the torque PI regulator is neglected when analyzing the torque ripple control loop. Furthermore, the stator voltage is considered as the disturbance term that is also ignored in the torque ripple control loop. Thus, The block diagram of the closed-loop control system based on an improved RC regulator is shown in Fig. 11, where $G_P(s) = 1/(R_r + \sigma L_r s)$ and $G_{PI}(s) = (K_{pi}s + K_{ii})/s$ are the corresponding functions of $G_p(z)$ and $G_{PI}(z)$ in the continuous domain, respectively, $G_d(z)$ is the delay plant, and $G_T = \psi_{sd} \cdot L_m/L_s$. The q-axis rotor current is applied for the average torque control. Thus, the output of the improved RC regulator is directly added to the q-axis rotor voltage reference.

As can be seen from the block diagram, the transfer function of the torque ripple closed-loop can be expressed as

$$G_{T_e}(z) = \frac{T_e}{T_e^*} = \frac{G_{IRC}(z)G_d(z)G_P(z)G_T}{1 + G_{PI}(z)G_d(z)G_P(z) + G_{IRC}(z)G_d(z)G_P(z)G_T}. \quad (29)$$

The denominator of (33), which is the characteristic polynomial of the overall improved RC-based closed-loop control system, can be written as

$$\Delta = 1 + G_{PI}(z)G_P(z)G_d(z) + G_{IRC}(z)G_P(z)G_TG_d(z) = (1 + G_{PI}(z)G_P(z)G_d(z))(1 + G_{IRC}(z)H(z)) \quad (30)$$

where $H(z)$ can be expressed as

$$H(z) = \frac{G_P(z)G_TG_d(z)}{1 + G_{PI}(z)G_P(z)G_d(z)}. \quad (31)$$

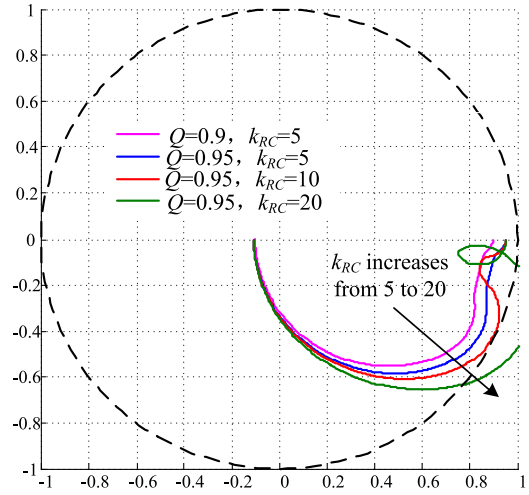

Fig. 12. Locus of the vector $S(z)$ with different bandwidths.

Assuming that the system is stable, the following inequality should be satisfied

$$\left[1 - (1 - k_{RC}G_{hp}(z)H(z))\,Qz^{-N_i}F(z)\right] \neq 0. \quad (32)$$

Expression (32) can be guaranteed if

$$|S(z)| = \left|(1 - k_{RC}G_{hp}(z)H(z))\,Qz^{-N_i}F(z)\right| < 1. \quad (33)$$

Fig. 12 shows the locus of the vector $S(z)$ with different Q and k_{RC}, in which constant Q is introduced for the bandwidth of the RC regulator. As can be seen from the figure, the decrease in the value of the constant Q is beneficial for the system stability and the increase in the gain k_{RC} will lead to the instability of the system. However, the constant Q cannot be too small because it will attenuate the gain of the improved RC regulator at the harmonic frequencies. Thus, the constant Q is 0.96 and the k_{RC} is chosen as 6 in the experimental system to guarantee the system stability.

B. Effectiveness of Improved RC Regulator

In order to validate the effectiveness of direct RC method in suppressing the torque ripple, the bode diagram of the transfer function (29) is plotted as shown in Fig. 13.

As can be seen from the bode diagram, when k_{RC} is equal to 4, 6, and 8, respectively, the magnitude response at 300 Hz are –0.14, –0.05, and 0 dB, respectively, and the phase response are all 0°. Thus, the increase in the gain k_{RC} is beneficial for the steady performance but also will introduce resonance that is harmful for the stability. In the experiments, k_{RC} is designed as 6, which is a tradeoff between the steady performance and system stability.

V. Experimental Results

In this part, the experimental results with the improved RC regulator disabled and enabled are shown to validate the proposed method. The schematic diagram of DFIG-based experimental system is shown in Fig. 14. The DFIG was driven by

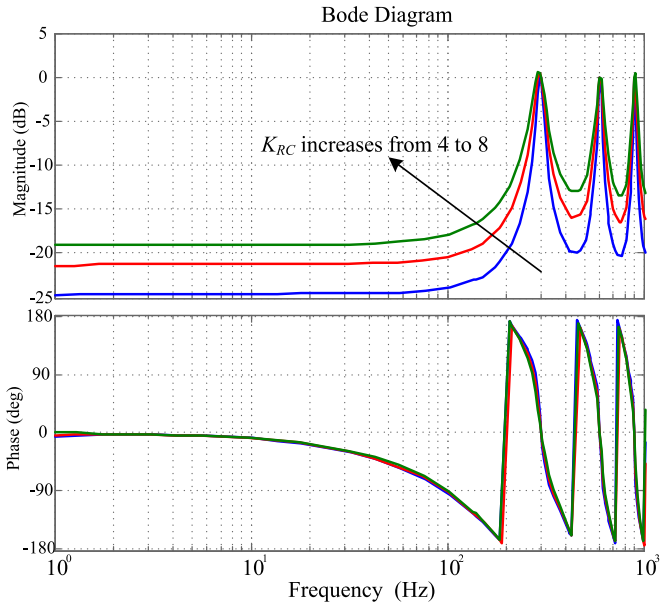

Fig. 13. Bode diagram of $G_{Te}(s)$ with k_{RC} variation.

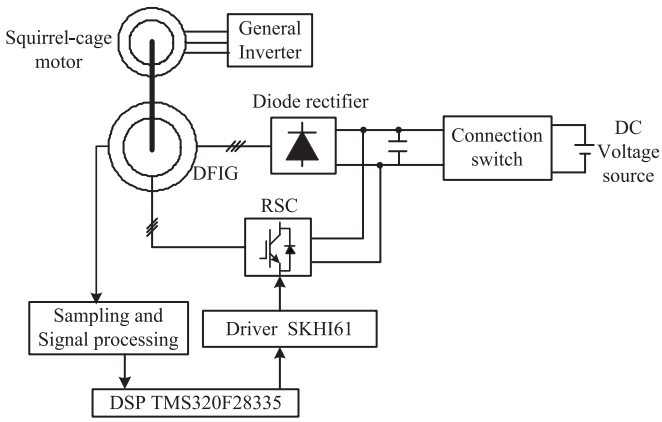

Fig. 14. Schematic diagram of the experiment system.

TABLE I
PARAMETERS OF THE TESTED DFIG

Parameters	*Value*	*Parameters*	*Value*
Rated power	1.0 kW	Rated voltage	110 V
Rated frequency	50 Hz	DC voltage	140 V
Stator/rotor turns ratio	0.33	R_s	1.01 Ω
R_r	0.88 Ω	L_m	87.5 mH
$L_{\sigma s}$	5.6 mH	$L_{\sigma r}$	5.6 mH

a squirrel cage induction motor with the control of general inverter. The control strategy of the RSC is implemented on the TI TMS320F28335 DSP and the switching frequency is 10 kHz with a sampling frequency of 10 kHz. The parameters of the DFIG are presented in Table I. All the waveforms are acquired by a YOKOGAWA DL750 scope.

Fig. 15 shows the steady-state experimental results of the DFIG system when the improved RC regulator is disabled.

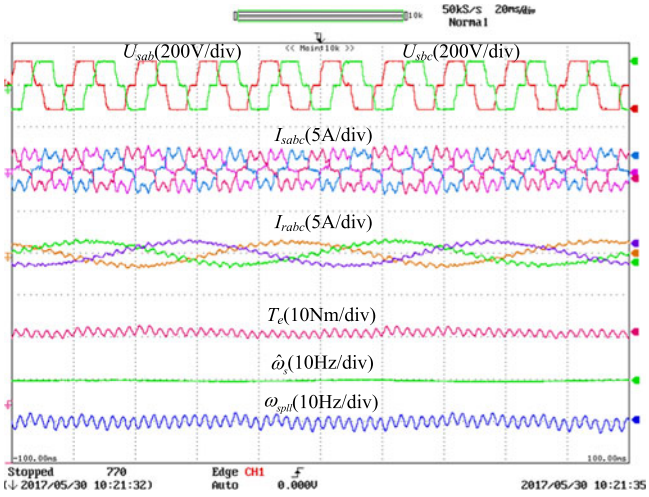

Fig. 15. Experimental results of a DFIG with improved RC disabled.

TABLE II
HARMONIC COMPONENTS IN STATOR VOLTAGE

Harmonic Order	5th	7th	11th	13th	17th	19th
Content	18.20%	11.73%	5.78%	4.12%	1.98%	1.67%

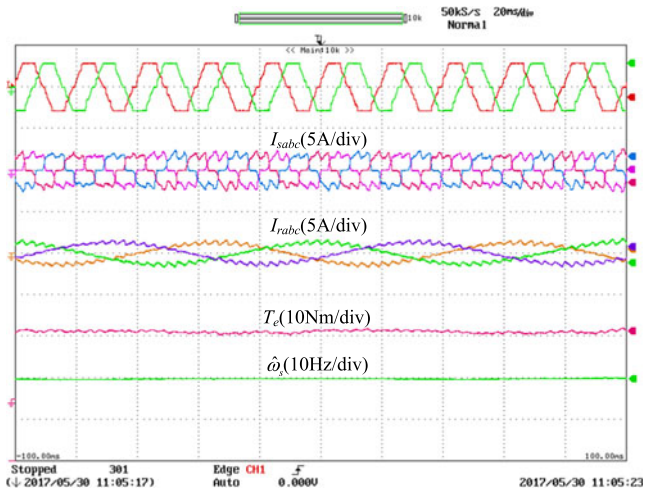

Fig. 16. Experimental results of a DFIG with improved RC enabled.

In the experimental tests, the torque reference is –4.775 N·m (–0.5 p.u.), and the stator power transferred to the dc voltage source is 500 W. The rotor speed is 800 r/min and the stator frequency is regulated to 50 Hz. The harmonic components of the stator voltage are presented in Table II, which indicates that high-order harmonic components are abundant in stator voltage. It is necessary to employ the improved RC regulator to suppress the torque ripple. The torque ripple is 0.45 N·m (9.4%). Furthermore, the estimated frequency $\hat{\omega}_s$ is very stable at 50 Hz. However, the frequency ω_{spll} obtained from conventional PLL is fluctuating around ±5 Hz.

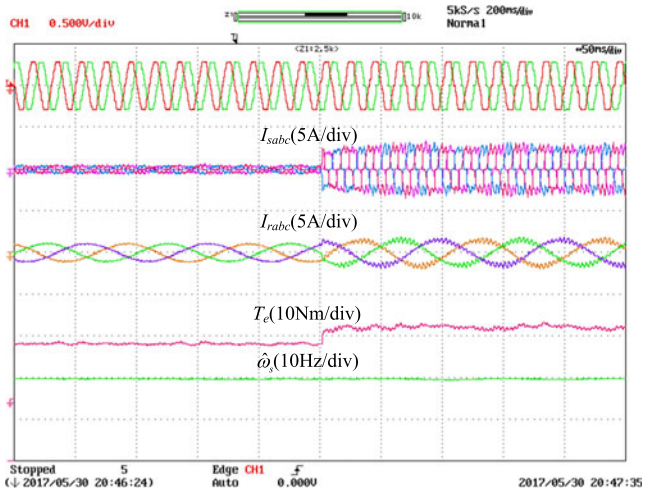

Fig. 17. Experimental results with the step response of a reference torque variation with improved RC enabled.

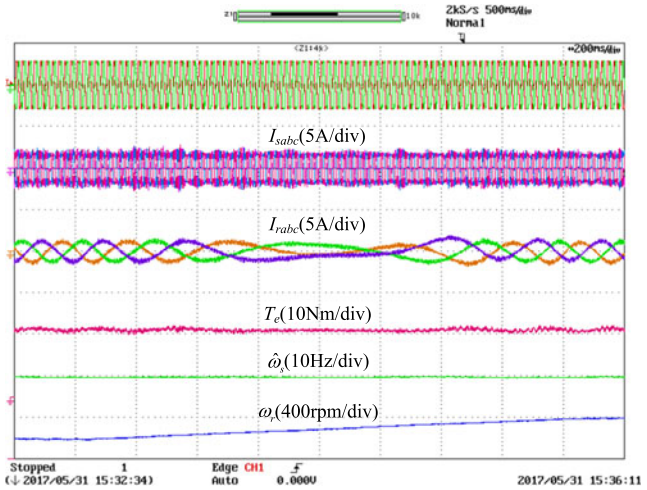

Fig. 18. Experimental results of DFIG showing the response of rotor speed variation with improved RC enabled.

Fig. 16 shows the steady-state experimental results of a DFIG system when the improved RC regulator is enabled, in which the operation condition is the same as Fig. 15. It can be seen that the torque ripple reduces to 0.02 N·m (0.4%), which is greatly suppressed. Thus, the improved RC regulator shows the satisfied performance in reducing the torque ripple. Furthermore, the stator frequency estimation is not influenced by the improved RC regulator.

Fig. 17 shows the experimental result showing the step response of a reference torque variation, in which the torque changes from –0.5 to –5.5 N·m. It can be seen that the electromagnetic torque rises to the reference torque just about 20 ms without any overshoot. During the step response of the electromagnetic torque, the estimated stator frequency is very stable without any fluctuation. As can be seen from the test result, the torque has a good dynamic response and the stator frequency is quite stable during the torque changing period.

Fig. 18 shows the experimental results when the rotor speed changes from 900 to 1100 r/min. The torque reference is set to –4.78 N·m and the improved RC regulator is enabled under this condition. The rotor current frequency changes from 5 to 0 Hz and to 5 Hz again. During the rotor speed changing period, the average value of torque is –4.8 N·m, which is approximately the same as the torque reference, and the stator power is around 500 W. The estimated stator frequency is not influenced by the rotor speed variation. The maximum torque ripple is 0.08 N·m during the rotor speed variation, which is also acceptable. It can be seen that the proposed control strategy can also achieve the stable operation capability of a DFIG system with rotor speed variation.

VI. Conclusion

In order to suppress the torque ripple of the DFIG-DC system, an improved RC regulator is proposed to directly produce appropriate harmonic voltages added to the rotor voltage reference. The torque control is divided into the average torque control and the torque ripple control. The specific contribution of this paper can be concluded as follows:

1) A novel PLL based on stator flux linkage is proposed for the decoupling control of the stator frequency and average torque. In this way, the distorted stator voltage is not needed anymore and the voltage sensors can be cancelled. As can be seen from the experimental results, the stator frequency is very stable, which is not influenced by the torque and rotor speed variation.
2) The high-order harmonic components in the torque ripple are all considered and an improved RC regulator is proposed to suppress the torque ripple completely.
3) The infinite dc gain of the conventional RC regulator is attenuated by the improved RC regulator. Thus, the direct resonant control can be applied for suppressing torque ripple without sequential separations and the complex rotor harmonic current calculations.

References

[1] U. Karaagac, J. Mahseredjian, L. Cai, and H. Saad, "Offshore wind farm modeling accuracy and efficiency in MMC-based multiterminal HVDC connection," *IEEE Trans. Power Del.*, vol. 32, no. 2, pp. 617–627, Apr. 2017.

[2] E. Muljadi, M. Singh, and V. Gevorgian, "Doubly fed induction generator in an offshore wind power plant operated at rated V/Hz," *IEEE Trans. Ind. Appl.*, vol. 49, no. 5, pp. 2197–2205, Oct. 2013.

[3] E. M. D. Miguel, S. M. David, A. Santiago, and D. C. Edgardo, "Optimal operation of offshore wind farms with line-commutated HVDC link connection," *IEEE Trans. Energy Convers.*, vol. 25, no. 2, pp. 71–78, Jun. 2010.

[4] R. Blasco-Gimenez, S. Anó-Villalba, J. Rodriguez-D'Derlée, S. Bernal-Perez, and F. Morant, "Diode-based HVDC link for the connection of large offshore wind farms," *IEEE Trans. Energy Convers.*, vol. 26, no. 2, pp. 615–626, Jun. 2011.

[5] H. Nian and X. Yi, "Coordinated control strategy for doubly-fed induction generator with DC connection topology," *IET Renewable Power Gener.*, vol. 9, no. 7, pp. 747–756, 2015.

[6] M. F. Iacchetti, G. D. Marques, and R. Perini, "Operation and design issues of a DFIG stator-connected to a DC-net by a diode rectifier," *IET Elect. Power Appl.*, vol. 8, no. 8, pp. 310–319, Sep. 2014.

[7] G. D. Marques and M. F. Iacchetti, "Stator frequency regulation in a field oriented controlled DFIG connected to a DC link," *IEEE Trans. Ind. Electron.*, vol. 61, no. 11, pp. 5930–5939, Nov. 2014.

[8] G. D. Marques and M. F. Iacchetti, "Inner control method and frequency regulation of a DFIG connected to a DC link," *IEEE Trans. Energy Convers.*, vol. 29, no. 2, pp. 435–444, Jun. 2014.

[9] G. D. Marques and M. F. Iacchetti, "Field-weakening control for efficiency optimization in a DFIG connected to a DC-Link," *IEEE Trans. Ind. Electron.*, vol. 63, no. 6, pp. 3409–3419, Jun. 2016.
[10] G. D. Marques and M. F. Iacchetti, "Air-gap power-based sensorless control in a DFIG connected to a DC link," *IEEE Trans. Energy Convers.*, vol. 30, no. 1, pp. 367–375, Mar. 2015.
[11] G. D. Marques and M. F. Iacchetti, "A self-sensing stator-current-based control system of a DFIG connected to a DC-Link," *IEEE Trans. Ind. Electron.*, vol. 62, no. 10, pp. 6140–6150, Oct. 2015.
[12] M. F. Iacchetti, G. D. Marques, and R. Perini, "Torque ripple reduction in a DFIG-DC system by resonant current controllers," *IEEE Trans. Power Electron.*, vol. 30, no. 8, pp. 4244–4254, Aug. 2015.
[13] H. Nian, C. Wu, and P. Cheng, "Direct resonant control strategy for torque ripple mitigation of DFIG connected to DC link through diode rectifier on stator," *IEEE Trans. Power Electron.*, vol. 32, no. 9, pp. 6936–6945, Sep. 2017.
[14] G. D. Marques and M. F. Iacchetti, "Minimization of torque ripple in the DFIG-DC system via predictive delay compensation," *IEEE Trans. Ind. Electron.*, to be published, doi: 10.1109/TIE.2017.2716860.
[15] H. Misra and A. K. Jain, "Analysis of stand-alone DFIG-DC system and DC voltage regulation with reduced sensors," *IEEE Trans. Ind. Electron.*, vol. 64, no. 6, pp. 4402–4412, Jun. 2017.
[16] A. Gundavarapu, H. Misra, and A. K. Jain, "Direct torque control scheme for DC voltage regulation of the standalone DFIG-DC system," *IEEE Trans. Ind. Electron.*, vol. 64, no. 5, pp. 3502–3512, May 2017.
[17] H. Misra, A. Gundavarapu, and A. K. Jain, "Control scheme for DC voltage regulation of stand-alone DFIG-DC system," *IEEE Trans. Ind. Electron.*, vol. 64, no. 4, pp. 2700–2708, Apr. 2017.
[18] Y. song and H. Nian, "Sinusoidal output current implementation of DFIG using repetitive control under a generalized harmonic power grid with frequency deviation," *IEEE Trans. Power. Electron.*, vol. 30, no. 12, pp. 6751–6762, Dec. 2015.
[19] Z. Zou, K. Zhou, Z. Wang, and M. Cheng, "Frequency-adaptive fractional-order repetitive control of shunt active power filters," *IEEE Trans. Ind. Electron.*, vol. 62, no. 3, pp. 1659–1667, Mar. 2015.
[20] D. Chen, J. Zhang, and Z. Qian, "Research on fast transient and $6n \pm 1$ harmonics suppressing repetitive control scheme for three-phase grid-connected inverters," *IET Power Electron.*, vol. 6, no. 3, pp. 601–610, 2013.
[21] D. Chen, J. Zhang, and Z. Qian, "An improved repetitive control scheme for grid-connected inverter with frequency-adaptive capability," *IEEE Trans. Ind. Electron.*, vol. 60, no. 2, pp. 814–823, Feb. 2013.
[22] Q. Zhao and Y. Ye, "A PIMR-type repetitive control for a grid-tied inverter: Structure, analysis, and design," *IEEE Trans. Power Electron.*, to be published, doi: 10.1109/TPEL.2017.2697939
[23] L. Fan, S. Yuvarajan, and R. Kavasseri, "Harmonics analysis of a DFIG for a wind energy conversion system," *IEEE Trans. Energy Convers.*, vol. 25, no. 1, pp. 181–190, Mar. 2010.

Chao Wu was born in Huanggang, China, in 1992. He received the B.Eng. degree in electrical engineering from the HeFei University of Technology, Hefei, China. He is currently working toward the Ph.D. degree in electrical engineering at Zhejiang University, Hangzhou, China.

His current research interests include the control strategy of doubly fed induction generators for dc power transmission in wind energy conversion systems.

Heng Nian (M'09–SM'14) received the B.Eng. and M.Eng. degrees from the HeFei University of Technology, Hefei, China, and the Ph.D. degree from Zhejiang University, Hangzhou, China, in 1999, 2002, and 2005, respectively, all in electrical engineering.

From 2005 to 2007, he was a Postdoctoral Researcher with the College of Electrical Engineering, Zhejiang University, China. In 2007, he was promoted as an Associate Professor. Since 2016, he has been a Full Professor at the College of Electrical Engineering, Zhejiang University. From 2013 to 2014, he was a Visiting Scholar with the Department of Electrical, Computer, and System Engineering, Rensselaer Polytechnic Institute, Troy, NY, USA. He has published more than 20 IEEE/IET Transaction papers and holds more than 20 issued/pending patents. His current research interests include the optimal design and operation control for wind power generation system.